ChemPubSoc Europe

DOI: 10.1002/cctc.201701306

CHEMCATCHEM Full Papers

Molybdenum Sulfide Nanosheet-Based Hollow Porous Flat Boxes and Nanotubes for Efficient Electrochemical Hydrogen Evolution

Liao Chen and Hongli Zhu*[a]

Intriguing amorphous/quasiamorphous molybdenum sulfide (MoS_x) materials with active terminal disulfide S_2^{2-} units have been recognized recently as prominent catalysts for the hydrogen evolution reaction (HER). Here, we diversify the MoS_x morphologies and structures by a facile template-free solvothermal method to prepare fascinating MoS_x nanosheet-based hollow porous flat boxes and nanotubes. As we increase the ethanol concentration in the mixed solvent for the reaction from 60 to 100 vol%, highly dispersed MoS_x materials are obtained and the morphologies change from nanosheet to nanosheet-based hollow porous nanotubes and ultimately to nanosheet-based hollow porous flat boxes with the increasing S_2^{2-} content. Catalytic measurements demonstrate that the hollow porous MoS_x flat boxes and nanotubes have similar outstanding HER performances and can reach 10 mA cm^{-2} current at overpotentials of approximately 206 and 210 mV, respectively.

Introduction

As a potential substitute for Pt, nonprecious molybdenum disulfide (MoS_2) materials have been developed to catalyze the hydrogen evolution reaction (HER). In addition to MoS_2 materials, amorphous/quasiamorphous molybdenum sulfide (MoS_x) materials[1] have been reported recently to be promising because of the exposed active sites from the intrinsically inert basal plane[2] and the unique disulfide (S_2^{2-}) units.[3] Although MoS_x materials have been the focus of plenty of investigations, the endeavors to endow them with regular morphologies and hierarchical structures are inadequate. Thanks to their limited anisotropy and good deformability, MoS_x materials have been deposited into 3D substrates/templates, the structures of which can be replicated and retained by the as-prepared MoS_x materials.[4] However, to date, almost no MoS_x materials with a self-supported regular morphology composed of hierarchical structures such as nanosheet-based hollow porous flat boxes and nanotubes have been reported. As the structure of a material is very important for its catalytic performance, it is of great significance and necessity to explore and exploit regular morphologies and hierarchical structures of MoS_x materials to extend their advantages.

Because MoS_x is similar to MoS_2 and may be considered as a precursor of MoS_2, research on MoS_2 materials with regular hierarchical structures can shed light on the preparation of MoS_x materials with unprecedented morphologies and structures. Initially, Feldman et al. confirmed the synthesis of MoS_2 fullerenes and nanotubes by a gas-phase reaction by virtue of the intermediate amorphous molybdenum trisulfide (MoS_3) phase obtained at elevated temperatures according to the ternary phase diagram of Mo–O–S.[5] After that, the merit of the intermediate amorphous MoS_3 phase was further proved and utilized by Nath et al. to develop a relatively simple thermal decomposition method of MoS_3 or MoS_3 precursors to prepare MoS_2 nanotubes.[6] Although these methods could be used to synthesize MoS_2 nanotubes and fullerenes, their applicability is restricted by the high reaction temperatures required and the nonhierarchical structures of the as-prepared MoS_2 fullerenes and nanotubes. Subsequently, liquid-phase methods have been developed to prepare nanosheet-based hierarchically structured MoS_2 nanotubes[7] and nanocages[8] with various templates under relatively mild conditions. Thanks to the hierarchical structures, nanosheet-based porous MoS_2 nanotubes and nanocages exhibited outstanding performances for hydrogen generation and lithium-ion battery anodes. Furthermore, porous MoS_2 nanotubes were also prepared without a template by the spontaneous self-assembly of MoS_2 nanosheets during growth in an ethanol-based mixed solvent under heating.[9] From previous studies on the preparation of MoS_2 materials with regular morphologies and hierarchical structures, it seemed that the amorphous MoS_3 precursor and the solvent component in the liquid-phase method were important factors to achieve regular hierarchical structures, although the mechanisms that influence this were not clear.

Inspired by the methods developed to prepare MoS_2 with regular morphologies and hierarchical structures, herein, for the first time, we have developed a facile template-free solvothermal method to synthesize MoS_x nanosheet-based hollow porous flat boxes and nanotubes by adjusting the ethanol content in the reaction solvent. In the process, MoS_x materials of low crystallinity and with characteristic S_2^{2-} units are akin to the intermediate amorphous MoS_3 during the preparation of

[a] L. Chen, Prof. H. Zhu
Department of Mechanical and Industrial Engineering
Northeastern University
Boston, MA 02115 (USA)
E-mail: h.zhu@northeastern.edu

Supporting information for this article can be found under: https://doi.org/10.1002/cctc.201701306.

MoS_2 nanotubes. At the same time, the presence of ethanol may help to facilitate and stabilize the assembly of MoS_x nanosheets at specific stages as reported previously.[9,10] After reaction, the as-synthesized MoS_x nanosheet-based hollow porous flat boxes are of 1–3 μm in length/width and 200–450 nm in thickness, and the nanotubes are several or more micrometers long with diameters of approximately 200–500 nm. For electrocatalytic hydrogen evolution, the MoS_x nanosheet-based hollow porous flat boxes and nanotubes both demonstrate outstanding performances, and the overpotentials to achieve 10 mA cm^{-2} current are approximately 206 and 210 mV, respectively.

Results and Discussion

If water is used as the solvent for the reaction of sodium molybdate dihydrate and thiourea in a sealed autoclave at 200 °C for 18 h, no observable solid substance is produced. However, if absolute ethanol is used instead of water, the outcome is completely different. A large amount of black product with excellent dispersity both in water and ethanol is obtained. As demonstrated by using SEM, the product is mainly hollow porous flat boxes with 2D nanosheets as building blocks (Figure 1a and b). As the synthesis is template free, the hollow porous flat boxes result from the self-assembly of nanosheets. The composition is measured by using energy-dispersive X-ray spectroscopy (EDS), and the results show that Mo and S atoms are distributed uniformly in the hollow porous flat boxes (Figure 1c–e). In Raman spectra, normally, the minor peak at $\tilde{\nu}=$ 404 cm^{-1} is an A_{1g} model Raman shift of semiconductor-phase MoS_2 (Figure 1f). However, the missing MoS_2 E^1_{2g} model peak and the emerging peak at $\tilde{\nu}=146$ cm^{-1} (Mo–Mo stretching vibration of metallic phase MoS_2) imply that the flat boxes have Raman features similar to that of metallic-phase MoS_2 to some degree.[11] The peak at $\tilde{\nu}=315$ cm^{-1} is assigned to the $\tilde{\nu}$(Mo–S) vibration that corresponds to the existence of bridging S_2^{2-} units.[1e,12] As the Raman spectra do not show clear peaks in the region of $\tilde{\nu}=520$–550 cm^{-1} in which the $\tilde{\nu}$(S–S) vibrations generally lie, we suppose that the S_2^{2-} units may not be dominant in the sample.[13] The composition and chemical states of the product are further confirmed by using X-ray photoelectron spectroscopy (XPS), and the result gives a Mo/S ratio of 1:2.72. By deconvolution, the characteristic high-resolution scan in the S 2p region can be fitted into two doublets (Figure 1g). One of the two doublets at a lower binding energy can be attributed to basal plane and apical S^{2-}, and the other doublet is caused by the existence of bridging and terminal S_2^{2-} as reported previously.[14] Therefore, highly dispersed MoS_x nanosheet-based hollow porous flat boxes have been synthesized by a template-free solvothermal method.

The crystallinity of the nanosheet-based hollow porous MoS_x flat boxes is obtained by using selected-area electron diffraction (SAED) in high-resolution transmission electron microscopy (HRTEM) and XRD. The nanosheets that compose the hollow porous flat boxes are observed clearly by using HRTEM (Figure 2a–d). The layer distance is 1.02 nm, which is larger than the classical MoS_2 layer distance (0.62–0.65 nm). Therefore

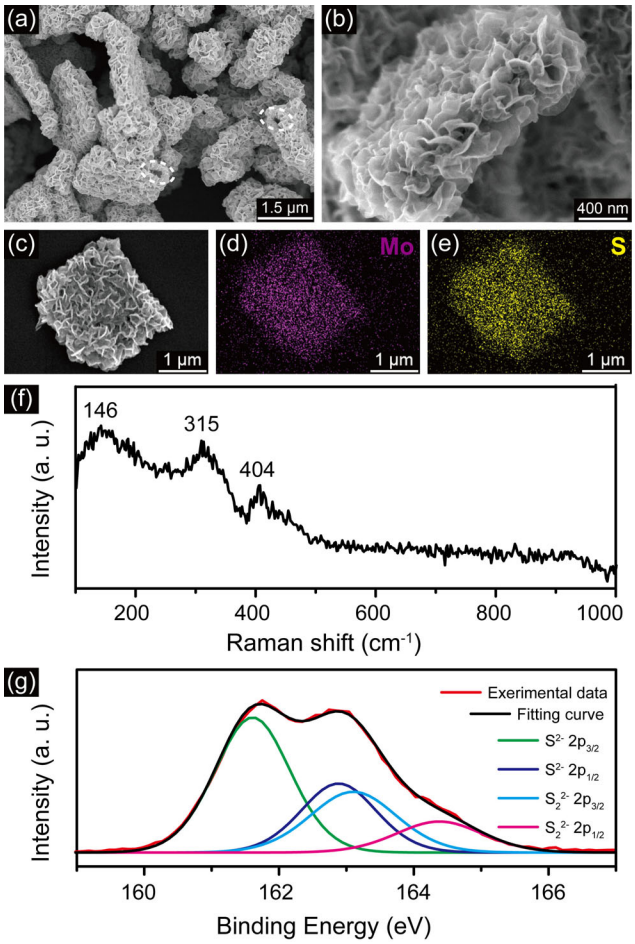

Figure 1. Morphology and composition of quasiamorphous MoS_x nanosheet-based hollow porous flat boxes: a,b) SEM images of the as-prepared MoS_x nanosheet-based hollow porous flat boxes (white circles in image a highlight the hollow internal structures); c–d) EDS results that show the uniform distribution of Mo and S atoms in the hollow porous flat box; f) Raman spectrum of MoS_x nanosheet-based hollow porous flat boxes; g) Deconvolution of the characteristic high-resolution XPS scan in the S2p region of the hollow porous flat boxes.

we conclude that the atomic layers in the nanosheets of flat boxes are packed loosely.[15] Although the fringes of the nanosheets show some kind of layer order, the SAED pattern of the flat box is broadened and blurry, which implies the imperfect order of the layers in the nanosheets and random arrangement of atoms in the layers as demonstrated by using HRTEM (Figure 2a and d). In addition, the powder XRD pattern of the product is quite similar to the patterns of amorphous/quasiamorphous MoS_x materials[16] (Figure 2e). The peak at $2\theta=8.7°$ originates from loosely packed layers in the nanosheets, and the calculated layer distance is 1.02 nm, which is consistent with the value obtained by using TEM. Accordingly, the as-prepared nanosheet-based hollow porous boxes are MoS_x with a low crystallinity and characteristic S_2^{2-} units.

As ethanol can help to produce the nanosheet-based hollow porous MoS_x flat boxes and ethanol is believed to have some impact on the self-assembly of nanosheets to form hierarchical MoS_2 structures,[9,10] the ethanol/water ratio in the solvent for the reaction is adjusted to check the influence of the ethanol

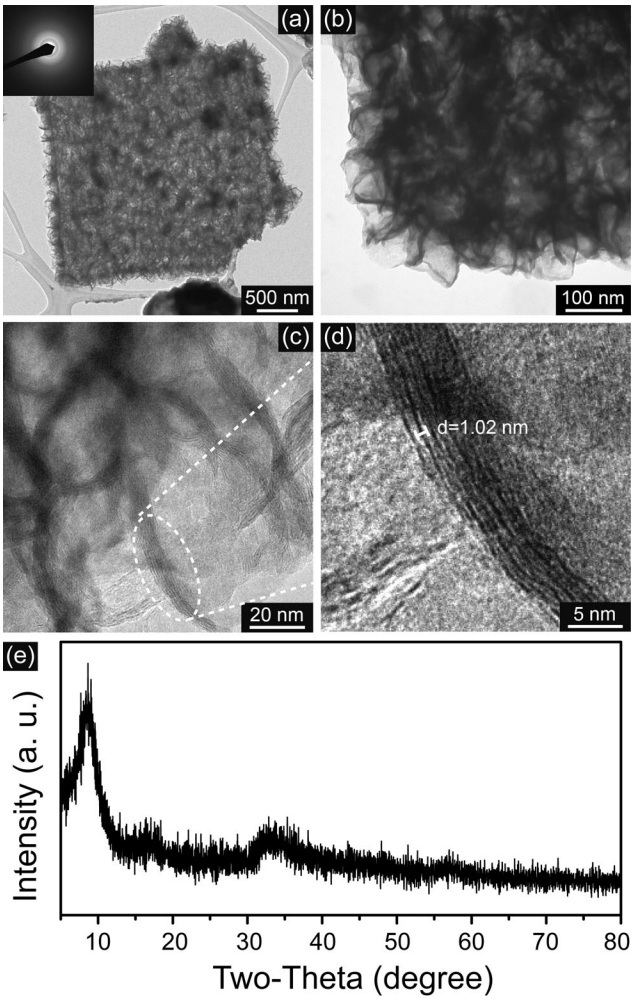

Figure 2. Crystallinity and assembly of as-prepared MoS_x nanosheet-based hollow porous flat boxes: a,b) TEM images of the nanosheet-based hollow porous flat boxes, the inset broadened and blurry SAED pattern in image a shows that the flat boxes have a low crystallinity; c,d) HRTEM images of the disordered atoms and loosely packed nanosheet layers in the hollow porous flat boxes; e) XRD pattern of the hollow porous flat boxes that indicates the loosely packed layers and poor crystallinity.

component on the formation of regular morphologies and hierarchical structures. Different from the situation if 100% ethanol is used, the product is mainly nanosheet-based hollow porous nanotubes intermingled with some nanosheets clusters if 80 vol% ethanol and 20 vol% water are used as the solvent for the reaction. The nanosheet-based hollow porous nanotubes have outside diameters of 200–500 nm and thicknesses of 50–70 nm as revealed by using SEM (Figure 3a and b) and TEM (Figure 3c and d). Again, as with the above flat boxes, the Mo and S atoms are distributed uniformly in the hollow porous nanotubes (Figure 3e–g). The XPS spectrum is used to calculate the Mo/S ratio, and the result is 1:2.54. In addition, the high-resolution scan in the S2p region is fitted into two doublets, and the doublet at higher binding energy is attributed to the characteristic bridging and terminal S_2^{2-} as for the above deconvolution of the S2p spectrum of hollow porous flat boxes (Figure S1a). The XRD pattern indicates that the

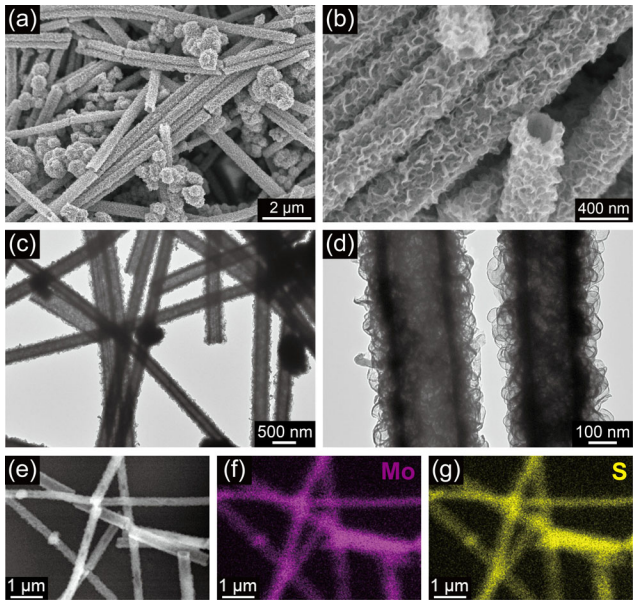

Figure 3. Morphology and composition of MoS_x nanosheet-based hollow porous nanotubes: a,b) SEM and c,d) TEM images of as-prepared MoS_x nanosheet-based hollow porous nanotubes; e–g) EDS results reveal the uniform distribution of Mo and S atoms in the hollow porous MoS_x nanotubes.

sample is poorly crystalline (Figure S1b). Therefore, MoS_x nanosheet-based hollow porous nanotubes are synthesized by adjusting the ethanol concentration in the reaction solvent conveniently.

If the nanosheet-based hollow porous flat box has structure regularity in two dimensions, then the nanosheet-based hollow porous nanotube has structure regularity only in one dimension. So, possibly, the regularity of the hierarchical structure of the product may have a positive correlation with the ethanol concentration in the reaction solvent. If the ethanol content is reduced to 60 vol%, the still highly dispersed product only consists of nanosheets and the randomly packed nanosheet structure actually has no structure regularity (Figure 4a and b). However, if the ethanol content is further reduced to 40 or 20 vol%, the products will become nondispersive and precipitate quickly and the apparent output decreases sharply (Figures S2 and S3). No solid product is harvested with pure water (0% ethanol) as the solvent for the reaction. The qualities and properties of the products prepared from low-ethanol-content solvents change dramatically and become clearly different from the highly dispersed products synthesized with high-ethanol-content solvents (Figures S3 and S4). Consequently, with 60 vol% ethanol in the reaction solvent, only MoS_x nanosheets are produced, and the nanosheets assemble randomly (Figure 4c). If the ethanol content increases to approximately 80 vol%, the formed MoS_x nanosheets can assemble gradually into 1D regular hollow porous nanotubes of various aspect ratios. If the ethanol concentration is increased all the way to 100%, the assembly of the MoS_x nanosheets will demonstrate more regularity and produce two-dimensionally regular hollow porous flat boxes with different aspect ratios.

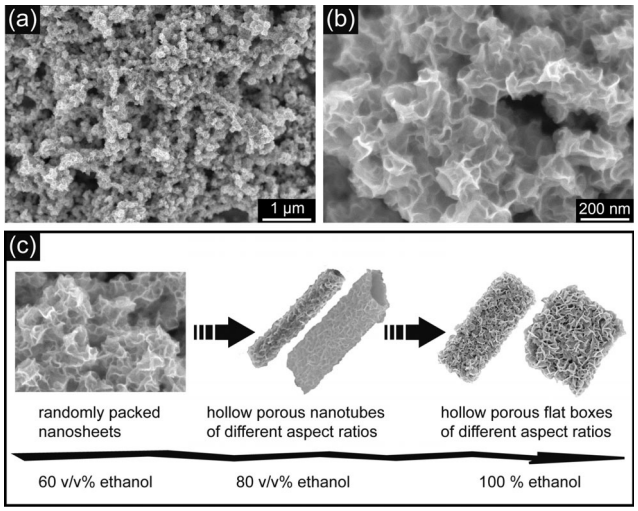

Figure 4. Highly dispersed nanosheets and the supposed assembly of the nanosheet-based regular structures: a,b) SEM images of randomly packed MoS_x nanosheets synthesized with a mixed solvent of 60 vol% ethanol; c) Representation of the assembly process of MoS_x nanosheets in the presence of different reaction solvents.

Although the ethanol content in the solvent can indeed influence the assembly of the nanosheets to form regular morphologies and hierarchical structures, the amorphous/quasiamorphous status of the intermediate phase or final product may also be an influential factor. Previously, amorphous MoS_3 has been an important intermediate phase in the formation of MoS_2 fullerene and nanotube structures.[5–6] Here, the highly dispersed nanosheets and nanosheet-based hollow porous nanotubes and flat boxes are in a quasiamorphous status between amorphous MoS_3 and crystalline MoS_2. Hence, the MoS_x has the ability to assemble and transform into regular and hierarchical structures. As the higher concentration of S_2^{2-} ensures the closer relationship of MoS_x with MoS_3, MoS_x materials with more S_2^{2-} may form fascinating structures. From the fitting of the high-resolution spectra in the S 2p region, the concentrations of S_2^{2-} of the three kinds of highly dispersed MoS_x materials are calculated (Table 1). As expected, the MoS_x nanosheet-based hollow porous flat boxes (100 vol% ethanol) have the highest S_2^{2-} concentration followed by the hollow porous nanotubes (80 vol% ethanol) and the randomly packed nanosheets (60 vol% ethanol) has the lowest S_2^{2-} concentration. For the particles prepared with a low ethanol concentration in the mixed solvent for the reaction, the XPS spectrum in the S 2p region will become totally different, and no S_2^{2-} units could be quantified from the high-resolution scan (Figure S4 b). We suppose that a specific concentration of ethanol in the reaction solvent can stabilize the MoS_x at a certain amount of S_2^{2-} units and meanwhile, the growing nanosheets would assemble under the influence of the existing ethanol (Figure 4 c). The more ethanol in the solvent for the reaction, the larger the amount of S_2^{2-} will be in the product and the more regular the hierarchical structure formed by the further assembly of the nanosheets. Other organic solvents for binary and ternary mixed solvents are under investigation to unravel the mechanisms of the influence of organic solvents on the S_2^{2-} amount and the assembly of nanosheets, and we believe the realization of a controllable amount of S_2^{2-} units and regular hierarchical structures may help us to prepare excellent MoS_x catalysts.

Table 1. Deconvolution and quantification of the high-resolution XPS scans in the S 2p region.

Sample	S^{2-} [eV]		S_2^{2-} [eV]		$S_2^{2-}/[S^{2-}+S_2^{2-}]$	S/Mo
	$2p_{3/2}$	$2p_{1/2}$	$2p_{3/2}$	$2p_{1/2}$		
MoS_x flat boxes	161.63	162.92	163.14	164.43	0.341	2.72
MoS_x nanotubes	161.63	162.90	163.14	164.40	0.274	2.54
MoS_x nanosheets	161.63	162.87	163.20	164.41	0.229	2.44

The intriguing MoS_x nanosheet-based hollow porous flat boxes and nanotubes are applied to catalyze the hydrogen evolution reaction with a classical three-electrode setup in 0.5 M H_2SO_4 solution. Unsurprisingly, the nanosheet-based hollow porous MoS_x flat boxes and nanotubes demonstrate excellent performances, and the required overpotentials to reach 10 mA cm^{-2} current are only approximately 206 and 210 mV, respectively, as indicated by the polarization curves (Figure 5 a). For comparison, highly dispersed randomly packed nanosheets are also tested, and the performance (≈215 mV overpotential

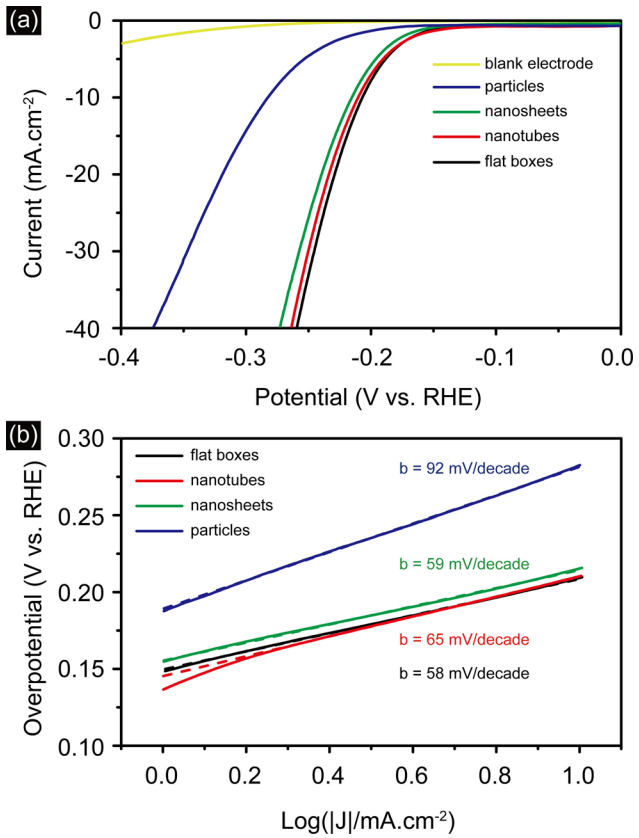

Figure 5. Electrocatalytic performances of the as-prepared MoS_x nanosheet-based hollow porous flat boxes, hollow porous nanotubes, nanosheets, and particles in the HER: a) Polarization curves that prove that the MoS_x nanosheet-based hollow porous flat boxes and nanotubes have similar superior HER performances; b) Tafel slopes obtained by the linear fitting of the Tafel regions from the corresponding polarization curves.

to achieve 10 mA cm^{-2} current) is slightly worse than that of the two hollow porous samples. This may be because of the increasing number of S_2^{2-} units and the increasing stability of nanosheets arrangements to expose sufficient active sites in the hollow porous samples with regular morphologies and hierarchical structures (Table 1 and Figures 1a and b, 3a and b, and 4a and b). In addition, the performances of the three highly dispersed nanosheets and nanosheet-based samples are significantly superior to that of the undispersed particles, which do not have the characteristic high-resolution S 2p spectrum that contains S_2^{2-} units (Figure S4b). The results indicate that a good amount of S_2^{2-} units, good material dispersity, and regular hierarchical structure stability are probably important factors to achieve excellent HER catalytic performances. Furthermore, Tafel slopes of the samples are obtained by the linear fitting of the polarization curves, and the Tafel slopes are quite similar and lie in the region of 58–65 mV/decade for the highly dispersed nanosheets and nanosheet-based samples. As for cycling stability, it seems that the two nanosheet-based hollow porous samples may be slightly more stable than the nanosheets sample (Figure S6). Accordingly, the MoS_x nanosheet-based hollow porous flat boxes and nanotubes have competitive catalytic performances (206–210 mV) and their performances are among the best (200–230 mV) of amorphous/quasiamorphous MoS_x materials prepared in the liquid phase under relatively convenient conditions.[1a,14a,17] Moreover, the nanosheet-based hollow porous MoS_x flat boxes and nanotubes may act as exceedingly effective supporters/templates to prepare other multifunctional catalysts.

Conclusion

We have synthesized MoS_x nanosheet-based hollow porous flat boxes and nanotubes by a facile template-free water/ethanol thermal method. With 60 vol% ethanol in the mixed solvent for the reaction, the highly dispersed black product consists of randomly packed nanosheets. As the ethanol concentration increases further, the components of the consistently highly dispersed products change from nanosheets to nanosheet-based hollow porous nanotubes and ultimately to nanosheet-based hollow porous flat boxes with increasing structural hierarchy/regularity. The presence of certain concentrations of ethanol may freeze the MoS_x in a quasiamorphous status with specific amounts of S_2^{2-} units and then the MoS_x nanosheets would grow and assemble into regular hollow porous nanotubes and flat boxes. The catalytic performances of MoS_x nanosheet-based hollow porous flat boxes and nanotubes in the hydrogen evolution reaction are outstanding, and the overpotentials to achieve 10 mA cm^{-2} current are approximately 206 and 210 mV, respectively. Therefore, nanosheet-based hollow porous MoS_x flat boxes and nanotubes are synthesized by a versatile water/ethanol thermal method, and the nanosheet-based hollow porous flat boxes and nanotubes can be used as synergistic supports/templates to prepare catalysts with heterostructures.

Experimental Section

Synthesis of MoS_x materials

For the synthesis of MoS_x nanosheet-based hollow porous flat boxes, sodium molybdate (20 mg; Sigma $\geq$ 99.5%) and thiourea (15 mg; Sigma $\geq$ 99.0%) were dispersed in ethanol (10 mL) by stirring for 1 h. The uniform suspension was transferred into a 25 mL PTFE-lined steel autoclave reactor, and the reactor was put into a 200 °C oven for 18 h. After reaction, the autoclave reactor was taken out to cool down naturally. The black dispersed MoS_x nanosheet-based hollow porous flat boxes product was obtained and washed with deionized water and ethanol each for at least three times.

For the synthesis of MoS_x nanosheet-based hollow porous nanotubes, sodium molybdate (20 mg) and thiourea (15 mg) were dissolved in a mixed solvent of ethanol (8 mL) and deionized water (2 mL). The transparent liquid was poured into a 25 mL PTFE-lined steel autoclave reactor. After heating at 200 °C for 18 h, the highly dispersed black product consisted of MoS_x nanosheet-based hollow porous nanotubes was produced. The product was washed with deionized water and ethanol each for at least three times.

With the same amount of reactants, if ethanol (6 mL) and deionized water (4 mL) was used as the solvent for the reaction in the autoclave reactor under 200 °C for 18 h, a highly dispersed black product of randomly packed nanosheets was harvested. If even less ethanol was applied in the mixed solvent for the reaction under the same conditions, only a small amount of undispersed product of particles was obtained. All the products were washed with deionized water and ethanol at least three times each.

Characterization

The morphologies and structures of the materials were imaged by using SEM (Hitachi SL4800) at 3 kV and by using HRTEM (JEOL 2010F). The atomic distribution was revealed by using EDS with SEM at a high voltage of 15 kV. SAED patterns were obtained by using the TEM setup. Crystallinity information was obtained by using powder XRD (PANalytical/Philips X'Pert Pro) with CuK_α radiation ($\lambda = 1.540598$ Å). The data was collected over $2\theta = 5$–$80°$ with a scan rate of 1° m^{-}. XPS spectra were measured by using a Thermo Scientific K-Alpha XPS system equipped with a monochromatic soft AlK_α X-ray source ($h\nu = 1.4866$ keV, line width ≈ 0.3 eV). To fit the high-resolution XPS curves in the Mo 3d and S 2p regions, the peak area ratio of each doublet was determined according to the degeneracy of the spin state. The binding energy separation of the doublet between $S\,2p_{3/2}$ and $S\,2p_{1/2}$ was (1.2 ± 0.1) eV. Raman spectroscopy was performed by using a LabRam HR800 with $\lambda =$ 532 nm laser excitation, and the samples were prepared by depositing the suspensions on silicon substrates.

Electrochemical measurements

A classical three-electrode setup with a working electrode (glassy carbon), a counter electrode (Pt plate), and a reference electrode (saturated calomel electrode; SCE) was used for the electrochemical measurements of the HER. The SCE reference electrode was calibrated by using a reversible hydrogen electrode (RHE). The calibration was conducted in H_2-saturated electrolyte, and the working electrode was a Pt wire. In 0.5 M H_2SO_4, $E(\mathrm{RHE}) = E(\mathrm{SCE}) + 0.31$ V, and all the potentials in this work were referenced to the RHE. All the samples were dispersed in a mixture of solvents (80 vol% deion-

ized water and 20 vol% ethanol) to prepare solutions of 1.32 mg mL^{-1} catalyst. Then, 20 μL of each suspension was dropped onto the 5 mm diameter glassy carbon electrode and dried under ambient conditions. Linear sweep voltammetry was performed at a scan rate of 3 mV s^{-1} in an electrolyte of 0.5 M sulfuric acid solution by using a Biologic potentiostat.

Acknowledgement

H.L.Z. acknowledges the financial startup support and Tier 1 award from Northeastern University. We also thank George J. Kostas Nanoscale Technology and Manufacturing Research Center at Northeastern University and Center for Nanoscale System at Harvard University for the use of their facilities. We thank Dr. Wentao Liang at Northeastern University for helping to perform HRTEM.

Conflict of interest

The authors declare no conflict of interest.

Keywords: electrocatalysis · hydrogen evolution reaction · molybdenum · nanostructures · nanotubes

[1] a) J. D. Benck, Z. B. Chen, L. Y. Kuritzky, A. J. Forman, T. F. Jaramillo, *ACS Catal.* **2012**, *2*, 1916; b) S. C. Lee, J. D. Benck, C. Tsai, J. Park, A. L. Koh, F. Abild-Pedersen, T. F. Jaramillo, R. Sinclair, *ACS Nano* **2016**, *10*, 624; c) D. Merki, S. Fierro, H. Vrubel, X. L. Hu, *Chem. Sci.* **2011**, *2*, 1262; d) C. G. Morales-Guio, X. L. Hu, *Acc. Chem. Res.* **2014**, *47*, 2671; e) P. D. Tran, T. V. Tran, M. Orio, S. Torelli, Q. D. Truong, K. Nayuki, Y. Sasaki, S. Y. Chiam, R. Yi, I. Honma, J. Barber, V. Artero, *Nat. Mater.* **2016**, *15*, 640; f) H. Vrubel, X. L. Hu, *ACS Catal.* **2013**, *3*, 2002.

[2] a) Y. P. Li, Y. F. Yu, Y. F. Huang, R. A. Nielsen, W. A. Goddard, Y. Li, L. Y. Cao, *ACS Catal.* **2015**, *5*, 448; b) D. N. Nguyen, L. N. Nguyen, P. D. Nguyen, T. V. Thu, A. D. Nguyen, P. D. Tran, *J. Phys. Chem. C* **2016**, *120*, 28789; c) J. F. Xie, Y. Xie, *ChemCatChem* **2015**, *7*, 2568.

[3] a) B. Lassalle-Kaiser, D. Merki, H. Vrubel, S. Gul, V. K. Yachandra, X. L. Hu, J. Yano, *J. Am. Chem. Soc.* **2015**, *137*, 314; b) L. R. L. Ting, Y. L. Deng, L. Ma, Y. J. Zhang, A. A. Peterson, B. S. Yeo, *ACS Catal.* **2016**, *6*, 861; c) C. L. Hsu, Y. H. Chang, T. Y. Chen, C. C. Tseng, K. H. Wei, L. J. Li, *Int. J. Hydrogen Energy* **2014**, *39*, 4788.

[4] a) Y. H. Chang, C. T. Lin, T. Y. Chen, C. L. Hsu, Y. H. Lee, W. J. Zhang, K. H. Wei, L. J. Li, *Adv. Mater.* **2013**, *25*, 756; b) K. C. Pham, Y. H. Chang, D. S. McPhail, C. Mattevi, A. T. S. Wee, D. H. C. Chua, *ACS Appl. Mater. Interfaces* **2016**, *8*, 5961; c) L. Chen, X. M. Geng, L. Yang, W. T. Liang, H. L. Zhu, *Int. J. Hydrogen Energy* **2017**, *42*, 26659.

[5] Y. Feldman, E. Wasserman, D. J. Srolovitz, R. Tenne, *Science* **1995**, *267*, 222.

[6] M. Nath, A. Govindaraj, C. N. R. Rao, *Adv. Mater.* **2001**, *13*, 283.

[7] a) C. P. Gu, W. M. Guan, Y. W. Cui, Y. Chen, L. L. Gao, J. R. Huang, *J. Mater. Chem. A* **2016**, *4*, 17000; b) G. D. Li, X. Y. Zeng, T. D. Zhang, W. Y. Ma, W. P. Li, M. Wang, *CrystEngComm* **2014**, *16*, 10754; c) J. Wang, J. L. Liu, H. Yang, Z. Chen, J. Y. Lin, Z. X. Shen, *J. Mater. Chem. A* **2016**, *4*, 7565; d) S. F. Zhuo, Y. Xu, W. W. Zhao, J. Zhang, B. Zhang, *Angew. Chem. Int. Ed.* **2013**, *52*, 8602; *Angew. Chem.* **2013**, *125*, 8764.

[8] a) X. Y. Yu, Y. Feng, Y. Jeon, B. Guan, X. W. Lou, U. Paik, *Adv. Mater.* **2016**, *28*, 9006; b) X. Y. Yu, H. Hu, Y. W. Wang, H. Y. Chen, X. W. Lou, *Angew. Chem. Int. Ed.* **2015**, *54*, 7395; *Angew. Chem.* **2015**, *127*, 7503; c) L. Zhang, H. B. Wu, Y. Yan, X. Wang, X. W. Lou, *Energy Environ. Sci.* **2014**, *7*, 3302; d) X. X. Zuo, K. Chang, J. Zhao, Z. Z. Xie, H. W. Tang, B. Li, Z. R. Chang, *J. Mater. Chem. A* **2016**, *4*, 51.

[9] P. P. Wang, H. Y. Sun, Y. J. Ji, W. H. Li, X. Wang, *Adv. Mater.* **2014**, *26*, 964.

[10] M. W. Xu, F. L. Yi, Y. B. Niu, J. L. Xie, J. K. Hou, S. G. Liu, W. H. Hu, Y. T. Li, C. M. Li, *J. Mater. Chem. A* **2015**, *3*, 9932.

[11] X. M. Geng, W. W. Sun, W. Wu, B. Chen, A. Al-Hilo, M. Benamara, H. L. Zhu, F. Watanabe, J. B. Cui, T. P. Chen, *Nat. Commun.* **2016**, *7*, 10672.

[12] T. Weber, J. C. Muijsers, J. W. Niemantsverdriet, *J. Phys. Chem.* **1995**, *99*, 9194.

[13] Y. L. Deng, L. R. L. Ting, P. H. L. Neo, Y. J. Zhang, A. A. Peterson, B. S. Yeo, *ACS Catal.* **2016**, *6*, 7790.

[14] a) R. Bose, S. K. Balasingam, S. Shin, Z. Jin, D. H. Kwon, Y. Jun, Y. S. Min, *Langmuir* **2015**, *31*, 5220; b) A. Y. Lu, X. L. Yang, C. C. Tseng, S. X. Min, S. H. Lin, C. L. Hsu, H. N. Li, H. C. Idriss, J. L. Kuo, K. W. Huang, L. J. Li, *Small* **2016**, *12*, 5530.

[15] a) M. R. Gao, M. K. Y. Chan, Y. G. Sun, *Nat. Commun.* **2015**, *6*, 7493; b) H. T. Wang, Z. Y. Lu, S. C. Xu, D. S. Kong, J. J. Cha, G. Y. Zheng, P. C. Hsu, K. Yan, D. Bradshaw, F. B. Prinz, Y. Cui, *Proc. Natl. Acad. Sci. USA* **2013**, *110*, 19701.

[16] a) Z. Z. Wu, D. Z. Wang, A. K. Sun, *J. Mater. Sci.* **2010**, *45*, 182; b) G. Nagaraju, C. N. Tharamani, G. T. Chandrappa, J. Livage, *Nanoscale Res. Lett.* **2007**, *2*, 461.

[17] a) X. B. Ge, L. Y. Chen, L. Zhang, Y. R. Wen, A. Hirata, M. W. Chen, *Adv. Mater.* **2014**, *26*, 3100; b) M. Guo, Q. Wu, M. Yu, Y. Wang, M. Li, *Electrochim. Acta* **2017**, *236*, 280; c) T. W. Lin, C. J. Liu, J. Y. Lin, *Appl. Catal. B* **2013**, *134*, 75.

Manuscript received: August 9, 2017
Revised manuscript received: September 19, 2017
Accepted manuscript online: September 21, 2017
Version of record online: ■■ ■■, 0000

Out of the box: We diversify MoS_x morphologies and structures by a facile template-free solvothermal method to prepare fascinating MoS_x nanosheet-based hollow porous flat boxes and nanotubes. Catalytic measurements demonstrate that the hollow porous MoS_x flat boxes and nanotubes have similar outstanding performances for the hydrogen evolution reaction and can reach 10 mA cm^{-2} current at overpotentials of approximately 206 and 210 mV, respectively.

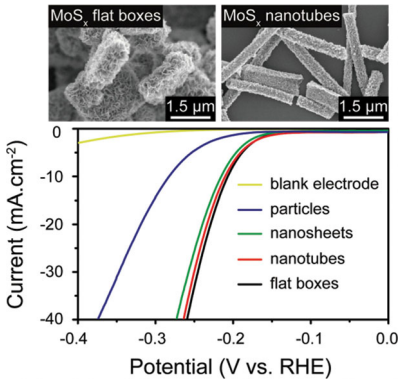

*L. Chen, H. Zhu**

■■ – ■■

Molybdenum Sulfide Nanosheet-Based Hollow Porous Flat Boxes and Nanotubes for Efficient Electrochemical Hydrogen Evolution